A Simplified Variable Admittance Controller Based on a Virtual Agonist-Antagonist Mechanism for Robot Joint Control

Xiaofeng Xiong, Florentin Wörgötter and Poramate Manoonpong

the Bernstein Center for Computational Neuroscience, Institute of Physics III, University of Göttingen, Göttingen, 37077 , Germany
E-mail: (xiong, worgott, poramate)@physik3.gwdg.de.

In this paper, we propose a simplified variable admittance controller applied to robot joint control. It is based on a virtual agonist-antagonist mechanism (VAAM) consisting of contractile and parallel elements (CEs and PEs). "Virtual" here means that every joint physically actuated by a standard servo motor can produce variably compliant motions as if it were driven by a pair of agonist and antagonist muscles. This makes it different from variable stiffness actuators (VSAs) with mechanically bulky and complex mechanisms. Moreover, the controller differs from other conventional PID admittance and variable admittance controllers since it only relies on force sensing at the end effector of robot rather than complex force/torque sensing of every joint. We have successfully implemented the controller on our hexapod robot which enables it to perform variable compliant behaviors, thereby reducing contact force and preventing leg damages when it is imposed with static or dynamical perturbation.

Keywords: Muscle model, variable admittance control, hexapod robot

1. Introduction

A friendly interaction with environments is a prerequisite of emerging robotic applications so as to achieve safety, adaptivity and compliance. This can be done by developing actuators[1] and controllers[2] with variable admittance/impedance, which have been applied to safe human-robot interactions[3] and adaptive assist devices.[4] Generally, variable admittance/impedance actuators are characterized by mechanically sophisticated structures while variable admittance/impedance controllers rely on force/torque sensing as inputs. In this paper, we propose a virtual agonist-

antagonist mechanism (VAAM)[b] for a simplified variable admittance controller. This novel controller endows the system with easily changing compliance by tuning stiffness and damper coefficients $[K, D]$ of the parallel elements (PEs) of the VAAM. This makes it more suitable for joint control of small robots in comparison with mechanically bulky and complex variable stiffness actuators (VSAs).[6–8] Moreover, this novel controller depends only on force sensing at the end effector rather than complex torque/force sensing at each joint as PID admittance controllers.[9] It also does not include desired states like standard variable admittance controllers.[4]

2. A Virtual Angonist-Antagonist Mechanism (VAAM)

In Fig. 1(a), a joint, physically actuated by a standard servo motor, is driven by the VAAM (i.e., $M1$ and $M2$). $M1$ and $M2$ mimic the function of agonist and antagonist muscles when confronted with an external load F_{ext}. The joint motions are excited by F_{ext} at the shank. O is the resting position of the shank. $M1$ and $M2$ consist of parallel and contractile elements (PE and CE). Each PE is modelled by a spring-damper system (see Fig. 1(b)). The passive forces $F^P_{(1,2)}$ created by $PE_{(1,2)}$ can be represented as:

$$F^P_{(1,2)} = K_{(1,2)}(l^P_{(1,2)} - l_0) + D_{(1,2)}(v^P_{(1,2)} - v_0), \tag{1}$$

where $l^P_{(1,2)}$ are the lengths of $PE_{(1,2)}$. $v^P_{(1,2)}$ are their velocities, and their initial values $[l_0, v_0]$ are equal to $[0.085, 0]$. $K_{(1,2)}$ and $D_{(1,2)}$ are stiffness and damper coefficients of $PE_{(1,2)}$, respectively. Here, we set $K_1 = K_2 = K$ and $D_1 = D_2 = D$.

The active force produced by the VAAM is the product of its activation α and length-velocity function $F(l_C, v_C)$. The active forces $F^C_{(1,2)}$ generated by $CE_{(1,2)}$ are represented as:

$$F^C_{(1,2)} = \alpha_{(1,2)} F(l^C_{(1,2)}, v^C_{(1,2)}), \tag{2}$$

where $l^C_{(1,2)}$ are the lengths of $CE_{(1,2)}$, and $v^C_{(1,2)}$ are their velocities. $\alpha_{(1,2)}$ are the functions of the $CE_{(1,2)}$ activation.

The total forces F^T_1 and F^T_2 are the sum of the passive and active forces produced by $M1$ and $M2$ respectively (derived from Eqs.(1) and (2)),

[b]In this paper the joint, physically actuated by a standard servo motor, is driven by a virtual agonist-antagonist mechanism. Its contractile and parallel elements (CEs and PEs) are simulated.

$$F_1^T = \underbrace{K(l_1^P - l_0) + Dv_1^P}_{F_1^P} + \underbrace{\alpha_1 F(l_1^C, v_1^C)}_{F_1^C}, \tag{3}$$

$$F_2^T = \underbrace{K(l_2^P - l_0) + Dv_2^P}_{F_2^P} + \underbrace{\alpha_2 F(l_2^C, v_2^C)}_{F_2^C}. \tag{4}$$

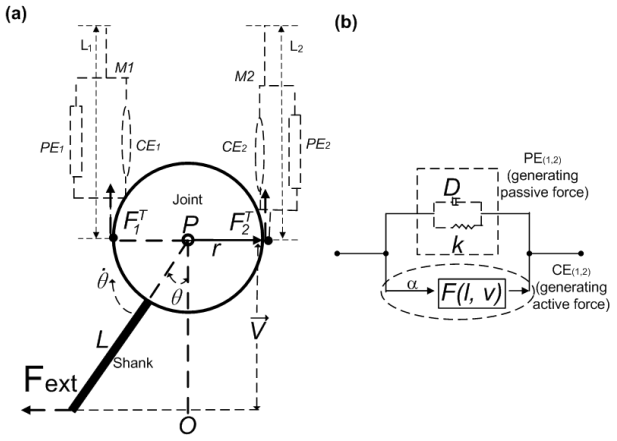

Fig. 1. The virtual agonist-antagonist mechanism (VAAM). (a) A joint driven by the VAAM. It consists of an agonist mechanism $M1$ and an antagonist mechanism $M2$ with lengths L_1 and L_2. Each of them consists of contractile and parallel elements (CE and PE). After applying force F_{ext} via a shank with length L to a joint P with the radius r, the joint angle θ changes. (b) The agonist and antagonist mechanisms $M1$ and $M2$. Their PEs (i.e. $PE_{(1,2)}$) producing passive forces are modelled as spring-damper mechanisms. Their CEs (i.e. $CE_{(1,2)}$) yielding active forces depend on their activation α and length-velocity function $F(l_C, v_C)$.

The antagonist mechanism $M2$ resists the extension of joint angle θ when it is excited by F_{ext}. Simultaneously, the agonist mechanism $M1$ produces opposing force against $M2$. Therefore, the direction of F_1^T is clockwise when the direction of F_2^T is counter-clockwise (see Fig. 1). According to the right-hand rule, the torque $\tau(F_2^T)$ direction points outward from the page. The torque $\tau(F_1^T)$ and $\tau(F_{ext})$ directions point into the page. We assume the torques pointing into the page to be positive. Then the torques $\tau(F_1^T)$,$\tau(F_2^T)$ and $\tau(F_{ext})$ acting on the joint P can be represented as:

$$\tau(F_1^T) = F_1^T r = (K(l_1^P - l_0) + Dv_1^P + \alpha_1 F(l_1^C, v_1^C))r, \tag{5}$$

$$\tau(F_2^T) = -F_2^T r = -(K(l_2^P - l_0) + Dv_2^P + \alpha_2 F(l_2^C, v_2^C))r, \tag{6}$$

$$\tau(F_{ext}) = F_{ext}\vec{V} = F_{ext}(L + r)\cos(\theta), \tag{7}$$

where $\vec{V}$ is the displacement vector of F_{ext} relative to the joint P. r is the radius of the joint P.

When applying Euler's laws of motion to the rotations of the joint P (see Fig. 1(a)), the net torque $\sum\tau$ acting on the joint P is equal to the product of its moment of inertia I and angular acceleration $\ddot{\theta}$,

$$I\ddot{\theta} = \sum\tau = \tau(F_{ext}) + \tau(F_1^T) + \tau(F_2^T). \tag{8}$$

Substituting Eqs.(5), (6) and (7) into Eq.(8), we obtain:

$$\begin{aligned} I\ddot{\theta} = {} & F_{ext}(L + r)\cos(\theta) \\ & + r[(K(l_1^P - l_0) + Dv_1^P + \alpha_1 F(l_1^C, v_1^C)) \\ & - (K(l_2^P - l_0) + Dv_2^P + \alpha_2 F(l_2^P, v_2^P))]. \end{aligned} \tag{9}$$

The lengths (i.e. $L_{(1,2)}$) of $M1$ and $M2$ are equal to the lengths of their CE and PE (i.e., $L_1 = l_1^P = l_1^C, L_2 = l_2^P = l_2^C$). In Fig. 1, $M1$ is shortening when $M2$ is lengthening. $\Delta L_{(1,2)}$ are the displacements of $M1$ and $M2$, i.e. $-(\Delta L_1) = \Delta L_2$. Here we postulate the relationship between their displacements $\Delta L_{(1,2)}$ and the joint angle θ,

$$-(\Delta L_1) = \Delta L_2 = \theta r = l_2^P - l_0 = -(l_1^P - l_0), \tag{10}$$

The relationship between velocities $\dot{\Delta L_{(1,2)}}$ and the joint velocity $\dot{\theta}$ can be represented as:

$$-\dot{\Delta L_1} = \dot{\Delta L_2} = \dot{\theta} r = v_2^P = -v_1^P. \tag{11}$$

Note that the initial values of $[v_1^P, v_2^P]$ are equal to zero. Substituting Eqs.(10) and (11) into Eq.(9), we obtain:

$$\begin{aligned} I\ddot{\theta} = {} & F_{ext}(L + r)\cos(\theta) \\ & + r[\underbrace{(\alpha_1 F(\phi_1, \phi_2) - \alpha_2 F(\phi_3, \phi_4))}_{\text{active force}} \\ & - \underbrace{(2K\theta r + 2D\dot{\theta} r)}_{\text{passive force}}], \end{aligned} \tag{12}$$

Equation (12) consists of the active and passive forces generated by $CE_{(1,2)}$ and $PE_{(1,2)}$, respectively.

Many physiological experiments have shown that the passive properties of muscles play a key role in animal joint stability when confronted with external perturbations.[10] Inspired by this finding for robotic joint control, we set the $M1$ and $M2$ activations α_1, α_2 from Eq.(12) to zero. Thus, we obtain:

$$I\ddot{\theta} = F_{ext}\vec{V} - 2r^2(K\theta + D\dot{\theta}), \vec{V} = (L + r)\cos(\theta). \tag{13}$$

According to Eq.(13), the VAAM relies on its passive properties (i.e. the parallel elements (PEs)) resulting in a variable admittance controller.

The variable admittance control based on the VAAM is applied to the hexapod robot AMOS-II (see Manoonpong et.al[11] for more detail) having three joints (TC-, CTr-, FTi- joints[a]) at each leg (see Fig.2 (a)). A pair of the virtual PEs excited by vertical loads is implemented on the CTr- and FTi- joints of AMOS-II, since the TC- joints of AMOS-II only allow for horizontal movements. Without force/torque sensing at each joint, some computational simplifications need to be made for the displacement vectors $\vec{V}_{(1,2)}$ at the joints $J_{(1,2)}$ caused by the external force F_{ext} . According to the leg kinematic configuration, the displacement vector $\vec{V}_1$ of the FTi- joint can be represented by (derived from Eq. (7)):

$$\vec{V}_1 = (L_F + r)cos(\theta_1). \tag{14}$$

The displacement vector $\vec{V}_2$ of the CTr- joint, on which F_{ext} indirectly acts can be approximated by :

$$\vec{V}_2 = (L_C + r)cos(\theta_2) + \vec{V}_1. \tag{15}$$

Note that similar simplified computations of displacement vectors can also be made for legs with complex structures.

The legs can move vertically when they are excited by F_{ext}, which are detected by the force sensors installed in the legs. Here the link lengths L_F and L_C are set as: $L_F = 0.065(m), L_C = 0.11(m)$. r is the joint radius, which is equal to $0.01(m)$.

The rotation matrix can be represented as (derived from Eq.(13)):

$$\ddot{\theta}_{(2\times2)}I_{(2\times1)} = F_{ext}\vec{V}_{(2\times1)} - 2r^2(\theta_{(2\times2)}K_{(2\times1)} + \dot{\theta}_{(2\times2)}D_{(2\times1)}), \tag{16}$$

[a]The thoraco-coxal (TC-) joint enables forward and backward movements, the coxa-trochanteral (CTr-) joint enables elevation and depression of the leg, and the femur-tibia (FTi-) joint enables extension and flexion of tibia.

where the acceleration matrix $\ddot{\theta}_{(2\times2)}$ and inertia matrix $I_{(2\times1)}$ can be written as:

$$\ddot{\theta}_{(2\times2)} = \begin{bmatrix} \ddot{\theta}_1 & 0 \\ 0 & \ddot{\theta}_2 \end{bmatrix}, I_{(2\times1)} = \begin{bmatrix} 5.0 \times 10^{-7} \\ 5.0 \times 10^{-7} \end{bmatrix}. \quad (17)$$

The displacement vector matrix $\vec{V}_{(2\times1)}$ is:

$$\vec{V}_{(2\times1)} = \begin{bmatrix} \vec{V}_1 \\ \vec{V}_2 \end{bmatrix}, \begin{matrix} \vec{V}_1 = (L_F + r)cos(\theta_1) \\ \vec{V}_2 = (L_C + r)cos(\theta_2) + \vec{V}_1 \end{matrix}. \quad (18)$$

The joint angle matrix $\theta_{(2\times2)}$, stiffness coefficient matrix $K_{(2\times1)}$, velocity matrix $\dot{\theta}_{(2\times2)}$ and damper coefficient matrix $D_{(2\times1)}$ are:

$$\theta_{(2\times2)} = \begin{bmatrix} \theta_1 & 0 \\ 0 & \theta_2 \end{bmatrix}, K_{(2\times1)} = \begin{bmatrix} K \\ K \end{bmatrix}, \dot{\theta}_{(2\times2)} = \begin{bmatrix} \dot{\theta}_1 & 0 \\ 0 & \dot{\theta}_2 \end{bmatrix} D_{(2\times1)} = \begin{bmatrix} D \\ D \end{bmatrix}. \quad (19)$$

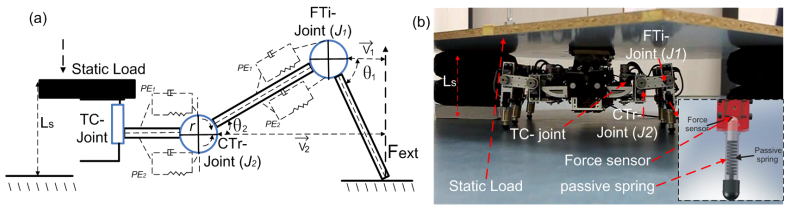

Fig. 2. Experimental model and setup. (a) AMOS-II leg with a simplified variable admittance controller (see Eq.(16)). The joints $J_{(1,2)}$ are driven by a pair of the virtual PEs, respectively. (b) AMOS-II is imposed with a static load (i.e. a white board).

3. Experimental results

In this setup (see Fig. 2 (b)), AMOS-II was placed between supporters (black wheels) having the total height of 18 cm (i.e. $L_s = 18(cm)$). Then a static load (i.e., a whiteboard) was placed on top of AMOS-II. It carried the full load, since its height (i.e. $22cm$) is higher than that of the supporters. The video clips of this experiment can be seen at http://www.manoonpong.com/CLAWAR2013/E1.wmv . When the FTi- and CTr- joints of AMOS-II are driven by the virtual PEs, it can automatically adapts its body height. Therefore, the legs with the virtual PEs suffer less contact force when AMOS-II is imposed with a static load. In contrast, without the virtual PEs, AMOS-II have to resist the load when the passive springs installed in the legs cannot be compressed anymore.

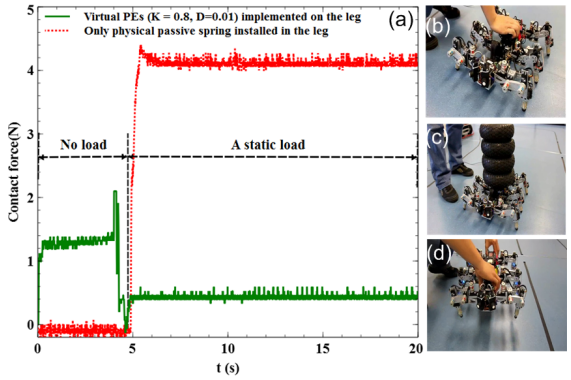

Fig. 3. (a)Comparison of the contact force arising with a static load. The force is measured at a foot contact sensor. (b) Hand pushing. (c) Placing a heavy load with a total weight of $5.72kg$. (d) Sudden Dropping (i.e. about ten centimetres).

Figures 3 (b)-(d) show experiments when AMOS-II was imposed with dynamical perturbations, like hand pushing, heavy load and sudden dropping. The video clips of these experiments can be seen at http://www.manoonpong.com/CLAWAR2013/E2.wmv . In hand pushing conditions, AMOS-II can produce 'softer' (i.e., $D = 0.001$) and 'stiffer' (i.e., $D = 0.1$) behaviors, by tuning the damper coefficients D in Eq.(16). However, these setups (i.e., $D = 0.001$ and $D = 0.1$) make AMOS-II unstable and suffer more contact force. Therefore, intermediately 'soft' (i.e., $D = 0.01$) was applied to AMOS-II when it was imposed with a heavy load and suddenly dropped. Overall, the PEs of the VAAM enable AMOS-II to perform variable compliant behaviors by tuning the damper coefficients D of its PEs. As a consequence, they make AMOS-II reduce contact force and prevent leg damages when it is imposed with static and dynamical perturbations. All stiffness coefficients K of its PEs were set to 0.8.

4. Conclusion

We presented a simplified variable admittance controller based on a virtual agonist-antagonist mechanism (VAAM). Two characteristics of this novel controller are: (1) through the simple tuning, this simplified variable controller can generate variable compliant behaviors without complex physical spring and damper mechanisms, e.g. variable stiffness actuators (VSAs), and (2) it also doesn't rely on complex force/torque sensing but rather simple force sensing at the end effector. The variable compliant behaviors are thereby produced by tuning the stiffness and damper coefficients (K, D) of

the PEs. These two characteristics enable robots to reduce contact force and generate variably 'soft'/'stiff' behaviors when receiving perturbations. In future work, the modular neural networks[11] will be used to control the CEs of the VAAM enabling AMOS-II to traverse different terrains with natural movements.

Acknowledgements: This research was supported by the Emmy Noether Program (DFG, MA4464/3-1), the Federal Ministry of Education and Research(BMBF) by a grant to the Bernstein Center for Computational Neuroscience II Göttingen (01GQ1005A, project D1), and European Communitys Seventh Framework Programme FP7/2007-2013 (Specific Programme Cooperation, Theme 3, Information and Communication Technologies) under grant agreement no. 270273, Xperience. We thank Martin Biehl, Guanjiao Ren and Frank Hesse for their discussions.

References

1. R. Ham, T. Sugar, B. Vanderborght, K. Hollander and D. Lefeber, *Robotics Automation Magazine, IEEE* **16**, 81 (september 2009).
2. C. Yang, G. Ganesh, S. Haddadin, S. Parusel, A. Albu-Schäffer and E. Burdet, *Robotics, IEEE Transactions on* **27**, 918 (oct. 2011).
3. S. Parusel, S. Haddadin and A. Albu-Schäffer, Modular state-based behavior control for safe human-robot interaction: A lightweight control architecture for a lightweight robot, in *Robotics and Automation (ICRA), 2011 IEEE International Conference on*, may 2011.
4. A. Lecours, B. Mayer-St-Onge and C. Gosselin, Variable admittance control of a four-degree-of-freedom intelligent assist device, in *Robotics and Automation (ICRA), 2012 IEEE International Conference on*, may 2012.
5. A. Albu-Schäffer, O. Eiberger, M. Grebenstein, S. Haddadin, C. Ott, T. Wimböck, S. Wolf and G. Hirzinger, *RAM, IEEE* **15**, 20 (september 2008).
6. M. Catalano, G. Grioli, M. Garabini, F. Bonomo, M. Mancinit, N. Tsagarakis and A. Bicchi, Vsa-cubebot: A modular variable stiffness platform for multiple degrees of freedom robots, in *Robotics and Automation (ICRA), 2011 IEEE International Conference on*, may 2011.
7. O. Eiberger, S. Haddadin, M. Weis, A. Albu-Schäffer and G. Hirzinger, On joint design with intrinsic variable compliance: derivation of the dlr qa-joint, in *Robotics and Automation (ICRA), 2010 IEEE International Conference on*, may 2010.
8. J. Hurst, J. Chestnutt and A. Rizzi, *Robotics, IEEE Transactions on* **26**, 597 (aug. 2010).
9. W. Yu, J. Rosen and X. Li, Pid admittance control for an upper limb exoskeleton, in *American Control Conference (ACC), 2011*, 29 2011-july 1 2011.
10. S. Sponberg and R. J. Full, *Journal of Experimental Biology* **211**, 433 (2008).
11. P. Manoonpong, U. Parlitz and F. Wörgötter, *Front. in Neural Circuits* **7** (2013).